Independent-atom-model description of multiple ionization of water, methane, and ammonia molecules by proton impact

Hans Jürgen Lüdde [*]
Center for Scientific Computing, Goethe-Universität, 60438 Frankfurt, Germany

Marko Horbatsch [†] and Tom Kirchner [‡]
Department of Physics and Astronomy, York University, Toronto, Ontario, Canada M3J 1P3

(Received 28 June 2022; accepted 17 August 2022; published 25 August 2022)

We study multiple ionization in proton collisions with water, methane, and ammonia molecules using an independent-atom model. Previous work on total (net) capture and ionization cross sections is extended to treat the multiple-ionization channels explicitly. We present the theoretical framework to treat charge-state correlated processes within the independent-atom-model approach, which uses the geometric screening introduced for different molecular geometries and orientations. A comparison of results is made for the target molecules H_2O, CH_4, and NH_3 with an emphasis on q-fold electron removal. Coincident measurements of produced molecular fragments can be used to estimate this quantity. We find very good agreement for the model calculations for the water molecule, where data exist for $q = 1$–4. For methane we observe reasonable agreement for $q = 1, 2$ and for ammonia only for $q = 1$, i.e., the experimental data show little support for a direct multiple-ionization channel in the latter case.

DOI: 10.1103/PhysRevA.106.022813

I. INTRODUCTION

The problem of electron removal from molecules impacted by charged particles has drawn considerable interest in recent years, chiefly because of its relevance in diverse fields ranging from atmospheric chemistry to biomedical applications [1]. In ion collisions, electron removal can be due to capture and ionization events and both can happen at the same time, giving rise to unstable multiply charged cations which undergo fragmentation. Experimental studies have looked at this problem in quite some detail, e.g., by measuring fragment ions in coincidence, whereas theoretical works have usually focused on more inclusive observables such as net capture and ionization cross sections, which are associated with the average number of electrons transferred from the target to the projectile or to the continuum. This is so because most theoretical approaches to the problem at hand are based on variants of effective one-electron treatments, and net cross sections are directly accessible in such a framework. If the projectile is singly charged, i.e., a proton, these net cross sections have often been equated with single-electron capture and ionization cross sections by virtue of interpreting the effective one-particle calculation as a single-active electron model description. This normally introduces but a small error in the single- or net-electron processes studied, but amounts to ignoring multiple ionization altogether and consequently leaves a sizable share of the accumulated experimental data unexplained.

In earlier work concerned with molecules such as water (H_2O) and methane (CH_4), we have taken a different viewpoint: We interpreted the solutions of the single-particle Schrödinger equation for each initially populated molecular orbital (MO) in an independent-electron-model (IEM) framework (with limited geometries) and combined them either multinomially or by using a more sophisticated analysis based on determinantal wave functions to obtain probabilities and cross sections for multielectron processes in addition to the net cross sections which are simply obtained by summing up the contributions from all MOs [2,3]. Similar ideas to deal with the many-electron aspects of the problem were used in recent classical-trajectory Monte Carlo work [4].

In yet another approach we applied an independent-atom-model (IAM) framework to calculate net cross sections for ion collisions with H_2O, CH_4, and larger (bio)molecules [5–9]. The IAM for collisions is built on the idea that a cross section for a molecular target can be written as a linear combination of atomic cross sections. Its simplest incarnation is the additivity rule (labeled IAM-AR), according to which the net cross sections for electron capture and ionization to the continuum are simply the sums of the net cross sections of all the atoms that make up the molecule. In a more refined variant of the IAM weight factors are attached to each atomic cross section in order to allow for geometric overlap in the effective molecular cross section. We termed the latter pixel counting method (labeled IAM-PCM), since the overlapping cross-sectional areas are calculated using pixelization.

The objective of the present work is to extend the IAM-AR and IAM-PCM approaches in such a way that in addition to net cross sections, probabilities and cross sections for multielectron processes can be extracted from the calculations. This

[*] luedde@itp.uni-frankfurt.de
[†] marko@yorku.ca
[‡] tomk@yorku.ca

 ©2022 American Physical Society

extension, which is once again based on the IEM, is described in Sec. II. In Sec. III the results of this analysis are shown for proton collisions with H_2O, CH_4, and NH_3 (ammonia), which have the same number of electrons, and are compared with experimental data and, in the case of H_2O, also with our previous MO-based calculations [2]. The paper ends with some concluding remarks in Sec. IV.

II. THEORETICAL CONSIDERATIONS

A. IEM analysis of multiple-capture and -ionization events

We are interested in calculating probabilities and cross sections for multiple-capture and -ionization processes. The starting point of the discussion is the exact expression for the probability of capturing k and simultaneously ionizing l electrons of an N-electron system ($k+l \leqslant N$) [10]

$$P_{kl} = \binom{N}{k+l}\binom{k+l}{l}\int_{P^k I^l T^{N-k-l}} \gamma^N d^4x_1 \cdots d^4x_N. \quad (1)$$

In Eq. (1), $\gamma^N = \gamma^N(x_1, \ldots, x_N; t_f)$ is the N-particle density of the system taken at a final time t_f long after the collision and $\int d^4x_j$ is shorthand for integration over the spatial coordinates and summation over the spin states of the jth electron, i.e., x_j comprises space and spin coordinates. The spatial integrals are with respect to the characteristic subspaces $P, T, I = V - P - T$, which correspond to finding an electron bound to the projectile (P), the target (T), or released to the ionization continuum (I) after the collision.

Within the framework of the IEM, the N-particle density is given in terms of the one-particle density matrix. If exchange is included it reads

$$\gamma^N = \frac{1}{N!}\begin{vmatrix} \gamma^1(x_1,x_1) & \cdots & \gamma^1(x_1,x_N) \\ \vdots & \vdots & \vdots \\ \gamma^1(x_N,x_1) & \cdots & \gamma^1(x_N,x_N) \end{vmatrix}, \quad (2)$$

while in the Hartree approximation we have

$$\gamma^N = \frac{1}{N^N}\prod_{j=1}^{N}\gamma^1(x_j). \quad (3)$$

Using the latter, we obtain for the charge-state correlated probabilities

$$\begin{aligned} P_{kl}^{\mathrm{IEM}} &= \binom{N}{k+l}\binom{k+l}{l}\frac{1}{N^N}\left(\int_P \gamma^1(x)d^4x\right)^k\left(\int_I \gamma^1(x)d^4x\right)^l\left(\int_T \gamma^1(x)d^4x\right)^{N-k-l} \\ &= \binom{N}{k+l}\binom{k+l}{l}\frac{1}{N^N}\left(P_C^{\mathrm{net}}\right)^k\left(P_I^{\mathrm{net}}\right)^l\left(P_T^{\mathrm{net}}\right)^{N-k-l} = \binom{N}{k+l}\binom{k+l}{l}P_C^k P_I^l P_T^{N-k-l} \\ &= \binom{N}{k+l}\binom{k+l}{l}P_C^k P_I^l (1-P_C-P_I)^{N-k-l}. \end{aligned} \quad (4)$$

In this sequence of equations, P_x^{net} are the (fractional) net numbers of electrons which are captured ($x = C$), ionized to the continuum ($x = I$), or which remain bound to the target ($x = T$) after the collision, while $P_x = P_x^{\mathrm{net}}/N$ are the corresponding properly normalized probabilities, i.e., $P_x \leqslant 1$. Note that Eq. (4) corresponds to an IEM analysis of capture and ionization in which shell-specific information is either unavailable or averaged out. It has been used in a large number of ion-atom collision studies (see, e.g., Refs. [11,12] and references therein).

B. Multiple capture and ionization in ion-molecule collisions in the IAM and IEM frameworks

We are interested in applying Eq. (4) to molecular targets:

$$\begin{aligned} &P_{kl}^{\mathrm{mol|IEM}}(E,b,\phi|\alpha,\theta,\varphi) \\ &= \binom{N}{k+l}\binom{k+l}{l}P_{C|\mathrm{mol}}^k P_{I|\mathrm{mol}}^l (1-P_{C|\mathrm{mol}}-P_{I|\mathrm{mol}})^{N-k-l}. \end{aligned} \quad (5)$$

In Eq. (5), E is the kinetic energy of the projectile (in the laboratory system), $\mathbf{b} = (b,\phi)$ is the impact parameter vector decomposed in polar coordinates, and α, θ, and φ are the Euler angles for the orientation of the target molecule in the z-y-z convention [13]. Within the IAM the molecular net probabilities are given as linear combinations of their $j = 1, \ldots, M$ atomic counterparts. In the IAM-AR framework one obtains the net numbers for processes $x = I, C, T$ simply by summing up the atomic net numbers. The IAM-PCM approach, on the other hand, includes weight factors in this summation, which account for the geometric overlap of the atomic cross sections when viewed from the perspective of the impinging projectile. Using these ideas, one obtains for the molecular probabilities on the right-hand side of Eq. (5),

$$P_{x|\mathrm{mol}}^{\mathrm{AR}} = \frac{1}{N}\sum_{j=1}^{M} P_{x|j}^{\mathrm{net}}(E,b_j) \quad (6)$$

and

$$P_{x|\mathrm{mol}}^{\mathrm{PCM}} = \frac{1}{N}\sum_{j=1}^{M} s_{x|j}(E|\alpha,\theta,\varphi)P_{x|j}^{\mathrm{net}}(E,b_j). \quad (7)$$

In Eq. (7), the coefficient $0 \leqslant s_{x|j} \leqslant 1$ is the weight factor for capture or ionization from the jth atomic constituent and $P_{x|j}^{\mathrm{net}}$ [cf. Eq. (6)] is the corresponding net electron number for a collision with that atom, which is located at $\mathbf{r}_j$ (assuming the molecule is in its ground-state configuration) such that $b_j = |\mathbf{b} - \mathbf{r}_j|$ is the atomic impact parameter.

With the Cartesian coordinates in the impact parameter plane $x_b = b\cos\phi$ and $y_b = b\sin\phi$, one has for a given orientation of the molecule (see Fig. 1) $b_j = \sqrt{(x_b - x_j)^2 + (y_b - y_j)^2}$. If the coordinates $\bar{x}_j$, $\bar{y}_j$, and $\bar{z}_j$

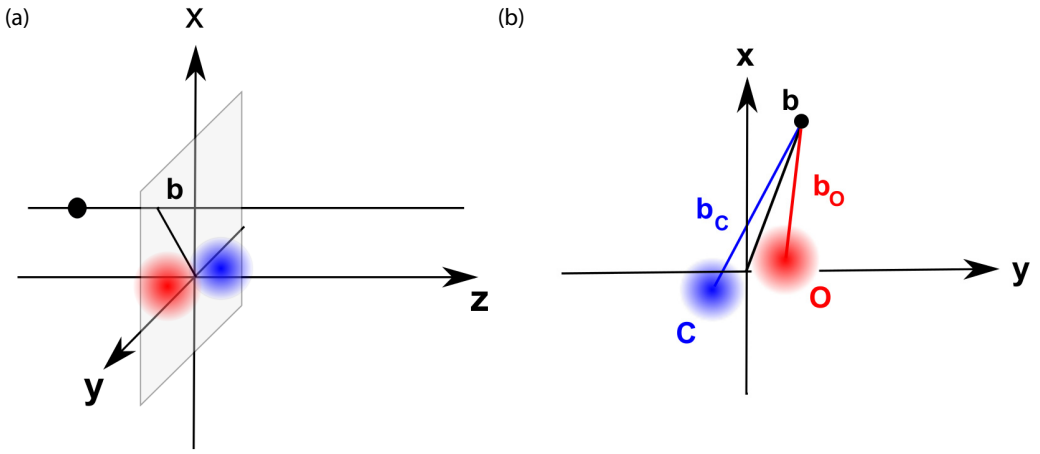

FIG. 1. (a) Scattering geometry and (b) projection on the impact parameter plane for a collision involving the CO molecule as an example.

refer to a fixed molecular frame with respect to which the structure information of the molecule is given, one obtains for the coordinates in the scattering frame, i.e., the coordinate system depicted in Fig. 1(a),

$$\begin{pmatrix} x_j \\ y_j \\ z_j \end{pmatrix} = \begin{pmatrix} \cos\alpha\cos\theta\cos\varphi - \sin\alpha\sin\varphi & \sin\alpha\cos\theta\cos\varphi + \cos\alpha\sin\varphi & \sin\theta\cos\varphi \\ -\cos\alpha\cos\theta\sin\varphi - \sin\alpha\cos\varphi & \cos\alpha\cos\varphi - \sin\alpha\cos\theta\sin\varphi & -\sin\theta\sin\varphi \\ -\cos\alpha\sin\theta & -\sin\alpha\sin\theta & \cos\theta \end{pmatrix} \begin{pmatrix} \bar{x}_j \\ \bar{y}_j \\ \bar{z}_j \end{pmatrix}. \tag{8}$$

Total cross sections for a given orientation of the molecule are obtained by integration over the impact parameter vector

$$\sigma_{kl}^{\mathrm{mol|IEM}}(E|\alpha,\theta,\varphi) = \int_0^{2\pi} d\phi \int_0^{\infty} b\,db\,P_{kl}^{\mathrm{mol|IEM}}(E,b,\phi|\alpha,\theta,\varphi). \tag{9}$$

Averaging over all orientations yields cross sections

$$\bar{\sigma}_{kl}^{\mathrm{mol|IEM}}(E) = \frac{1}{8\pi^2}\int_0^{2\pi} d\varphi \int_0^{\pi} \sin\theta\,d\theta \int_0^{2\pi} d\alpha\,\sigma_{kl}^{\mathrm{mol|IEM}}(E|\alpha,\theta,\varphi), \tag{10}$$

which are to be compared with experimental data obtained for randomly oriented molecules, i.e., they are the quantities of interest in this work.

C. Inclusive probabilities

The definition of the IEM probabilities ensures proper normalization

$$\sum_{k,l=0}^{k+l\leqslant N} P_{kl}^{\mathrm{IEM}} = 1. \tag{11}$$

In addition, the P_{kl}^{IEM} satisfy sum rules for q-fold capture and ionization

$$P_q^{C|\mathrm{IEM}} = \sum_{l=0}^{N-q} P_{ql}^{\mathrm{IEM}}, \tag{12}$$

$$P_q^{I|\mathrm{IEM}} = \sum_{k=0}^{N-q} P_{kq}^{\mathrm{IEM}}, \tag{13}$$

and they sum up to yield the corresponding net electron numbers

$$P_x^{\mathrm{net}} = \sum_{q=1}^{N} qP_q^{x|\mathrm{IEM}}. \tag{14}$$

We modify the probabilities and cross sections contributing to net capture according to

$$\tilde{\sigma}_{1q} = \sum_{k=1}^{N-q} k\sigma_{kq}, \tag{15}$$

$$\tilde{\sigma}_{k>1q} = 0 \tag{16}$$

in order to deal with the problem that the IEM inevitably produces nonzero probabilities for all $k+l \leqslant N$ combinations, regardless of whether the given projectile can accommodate k electrons. This pragmatic reinterpretation of multiple-capture events as contributors to single-capture processes was also used in our previous MO-based work [2]. We note that double capture ($k=2$) *can* occur for a proton projectile. However, it is such a rare and highly correlated process (associated with the formation of a negatively charged hydrogen ion) that in the context of the present IEM-based analysis it is considered unphysical and ruled out.

III. RESULTS AND DISCUSSION

The results reported in this work are based on the same two-center basis generator method (TC-BGM) [14] calculations for the $p+\mathrm{H}$, $p+\mathrm{C}$, $p+\mathrm{N}$, and $p+\mathrm{O}$ ion-atom systems as our previously published IAM-AR and IAM-PCM net cross sections [6,7]. In the present work we focus on IAM-PCM results and note that they go over into the additivity

rule limit at the highest energies, i.e., above 1 MeV. The TC-BGM is a coupled-channel method implemented at the IEM level of density-functional theory. Ground-state Hartree screening and exchange effects are treated exactly, while time-dependent variations are known to be of minor importance for proton collisions and are neglected. Further details are provided, e.g., in Ref. [5].

A. $p + H_2O$ collisions

We begin the discussion of results with a look at the $p + H_2O$ system, which we studied using an MO-based IEM framework in previous works [2,15,16]. The IAM-PCM net capture cross sections were discussed in detail in Ref. [8], where a comparison with other calculations was also provided.

We focus on charge-state correlated cross sections in this work, but start with the inclusive process of q-fold electron removal from water molecules. Experimental data can provide mostly estimates, since the measurements are not complete in terms of recording all coincidences. At intermediate energies (100–350 keV), for which capture processes play a role only at the lower end of the range, multiple electron removal cross sections for $q = 1$–4 can be derived from ionized fragment coincidence measurements reported in Ref. [17] (see Ref. [15]). Subsequent measurements at lower energies reported singly ionized fragment data [18,19]. In Ref. [19] higher-energy data from a separate measurement were reported and these were repeated more recently with emphasis on double ionization at high energies by reporting also coincident fragment yields [20]. Many of these measurements are incomplete in the sense that not all possible reaction channels were recorded, and this is why they provide typically lower bounds for q-fold electron removal. One of the difficulties one is faced with concerns the absolute normalization of the data, which in some cases is obtained by using the measured net cross sections for total electron production $\sigma^- = \sigma_{\rm ion}^{\rm net}$ and for total ion production $\sigma^+ = \sigma_{\rm ion}^{\rm net} + \sigma_{\rm cap}^{\rm net}$ [21].

These channels have been partially explained by the IEM calculations of Refs. [2,15], but the $q = 3$ channel was found to be overestimated already. Thus, it will be of interest to explore the success of the IAM-PCM approach.

Other theoretical approaches for collisions with water molecules with attempts to describe charge-state correlated cross sections include quantum treatments using continuum distorted wave approaches [22–24] as well as classical-trajectory calculations with model potentials [25]. These approaches have also been used to describe the ionized electron differential cross sections, but we have not found comparisons with the q-fold electron removal data of Werner *et al.* [17], which were derived in Ref. [15]. In principle, a promising approach in this respect might be the N-particle classical trajectory approach [26]. We note, however, that total cross sections cannot be obtained reliably from classical calculations due to their shortfall in describing ionization in distant collisions [27].

For the net electron removal process, experimental data are available for a wider range of energies in Refs. [18,19] and are based on fragment yields without coincidence counting. The problem of absolute normalization does exist though, since efficiencies for the detection of fragments are difficult to determine. The more recent measurements of Tavares *et al.* [20] were normalized by using a model curve that fits net recoil ion production [21], i.e., σ^+. In principle, such a procedure may be questioned on account of neglecting fragments with charges $q \geqslant 2$ and may assign slightly too high cross sections for the production of singly charged ions. At high energies, however, the observed cross sections for such channels are known to be small [17]. It is worth noting that this normalization procedure affects the H_2O^+ channel of the data, where the results from Ref. [20] are consistently higher than those of Ref. [19].

Apart from overall normalization, the data of Ref. [20] allow us to determine the relative yields of singly ionized fragments at intermediate to high energies in order to establish whether they follow the expected ratios of 68:16:13:3 for the fragments H_2O^+:OH^+:H^+:O^+ from photofragmentation [28]. The data from Ref. [20] do support these ratios with an accuracy of a few percent. This allows one to estimate the $q = 1$ production by dividing the normalized H_2O^+ cross section by about 0.68, which should be valid at least at high energies. The data of Ref. [19] were previously compared with theoretical MO IEM calculations in Refs. [2,15].

The IAM-PCM data are presented in Fig. 2. The curves at the top of Fig. 2(a) allow one to compare the net removal cross section σ^+ with the experimental fragmentation data of Refs. [17–20]. The most recent data at higher energies are those of Ref. [20] and are on the high side. The data of Ref. [17] were normalized by a different procedure at $E = 350$ keV and their net cross sections fall below these results for σ^+ for $E > 200$ keV. Concerning the magnitude of the net ionization cross section of Ref. [21], we note that other quantum-mechanical theoretical works fall below it at high energies, such as Refs. [22,23], with the exception of Ref. [24]. It can be seen that the IAM-PCM results fall a bit short in the 30–150 keV energy range (at about the 20% level) relative to the MO IEM data of Ref. [2], which were previously shown to match the experimental data quite well.

From a theoretical perspective the q-fold electron removal cross sections represent an inclusive quantity, as outlined in Sec. II. Charge-state correlated cross sections σ_{0l} and $\tilde{\sigma}_{1l}$ are calculated and then added correspondingly, i.e.,

$$\sigma_q = \tilde{\sigma}_{1q-1} + \sigma_{0q}. \tag{17}$$

The modified prescription for capture processes is used, i.e., Eq. (15), to avoid unphysical contributions from multiple-electron capture which otherwise would be obtained in an IEM.

For the $q = 1$ electron removal channel [short dashed lines in Fig. 2(a)] both the MO IEM and IAM-PCM methods show close agreement with each other, which is remarkable, since these are very different calculations. At low and intermediate energies their shape is different from that of the net cross section.

The comparison of the $q = 1$ channel with experimental data is provided separately in Fig. 2(b). The experimental data for the production of H_2O^+ molecular ions should be a lower bound for the $q = 1$ electron removal channel. The data at low to intermediate collision energies [18,19]

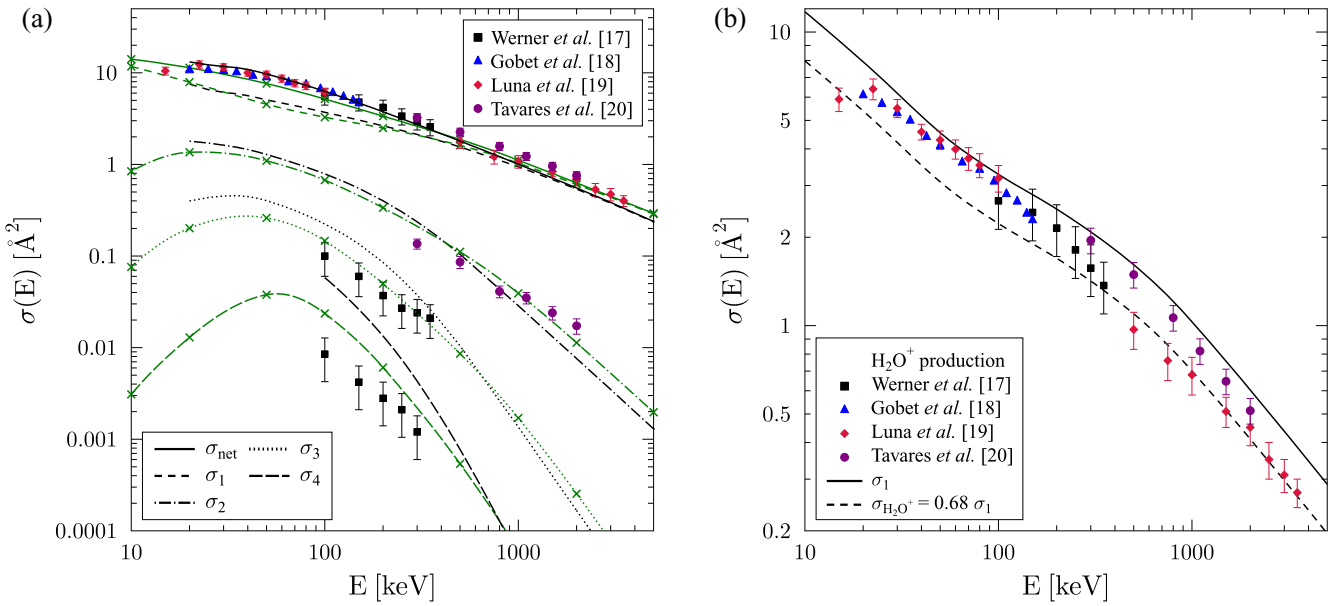

FIG. 2. Total cross sections for proton collisions with water molecules as functions of impact energy: (a) for net removal and $q = 1, 2, 3, 4$ charge-state production and (b) the case of $q = 1$ compared to the production of H_2O^+. In (a) the solid curves show the total (net) removal in the MO IEM (black, Ref. [16]) and IAM-PCM frameworks (green, marked with crosses, present work) in comparison to the fragmentation data of Werner *et al.* [17] (black squares), Gobet *et al.* [18] (blue triangles), Luna *et al.* [19] (red diamonds), and Tavares *et al.* [20] (purple circles). The broken lines are for $q = 1$ (short-dashed), $q = 2$ (dash-dotted), $q = 3$ (dotted), and $q = 4$ (long-dashed). The experimental data should be lower bounds for the q-fold electron removal cross sections (cf. the text). In (b) the legend for the experimental data for the production of H_2O^+ corresponds to those in (a), while the dashed line is the IAM-PCM estimate for this channel.

agree very well with each other and correspond well to the intermediate-energy results of Werner *et al.* [17]. The IAM-PCM data observe this bound very well. It is a tight bound at energies 30–100 keV, but we note that the modeling of fragmentation is not straightforward in this energy regime. The bound from the more recent higher-energy experimental data is very tight, which is a consequence of the data being normalized to those of Ref. [21]. The reason for the discrepancy between the data of Ref. [19] and the data of Ref. [20] has not been commented upon by the researchers, but we can assume that it is mostly related to the issue of different normalization.

At intermediate and high energies the fragmentation model which assumes $\sigma_1 \approx 0.68\sigma_{H_2O^+}$ can be trusted, since the fragment ratios approach constant values as a function of energy. The dashed curve in Fig. 2(b) shows that the IAM-PCM result agrees very well with the data of Ref. [19] and is consistent with those of Ref. [17], but less so with the more recent data of Ref. [20]. At energies below 100 keV where the results fall below those of Refs. [18,19] the fragmentation data are difficult to explain. We also note that a different fragmentation model has been proposed in the literature to find better agreement with the intermediate-energy fragmentation data (cf. [22]).

For the $q = 2$ channel both theoretical models shown as black and green dash-dotted lines (the latter with crosses) in Fig. 2(a) agree remarkably well with each other. In terms of a comparison with experiment for this inclusive cross section, one has again bounds based on some coincidence data. Werner *et al.* [17] reported coincidence measurements at energies of 100–350 keV that involved two protons in coincidence with neutrals or singly and doubly charged oxygen, but no coincidences between protons and OH^+. Tavares *et al.* [20], on the other hand, for the 300–2000 keV energy range, reported $H^+ + OH^+$ and $H^+ + O^+$ coincidences, but no $H^+ + H^+$ coincidences, so their data provide a lower bound for $q = 2$ production. Both theoretical models obey this bound for collision energies below 1000 keV, and if one were to add the $H^+ + H^+$ data at 300 keV from Ref. [17], one would get excellent agreement and have an almost complete comparison (assuming O^{2+} production with other neutral fragments is negligible).

At energies above 1000 keV the double-ionization data of Ref. [20] show a change in energy dependence which is consistent with the appearance of an autoionization contribution due to vacancy production in the $2a_1$ MO. We take the agreement of our model calculations with the experiment at lower energies as a strong indication that such processes are not required to understand the $q = 2$ production channel unless one moves up to higher collision energies where the $1/E^2$ falloff of the direct double-ionization process makes these autoionization contributions visible, since they scale with the $1/E$ energy dependence of the $2a_1$ vacancy production cross section.

For the $q = 3$ channel the coincidence data for the $H^+ + H^+ + O^+$ fragment yields of Ref. [17] provide a reasonable lower bound (assuming that the unobserved $H^0 + H^+ + O^{2+}$ channel is weak). The MO IEM lies above the experimental data by about a factor of 2, while the IAM-PCM results represent a good match at energies below 300 keV. The last two experimental data points indicate that for $q = 3$ autoionizing processes caused by $2a_1$ vacancies may

begin to contribute significantly at this three times lower energy compared to the case of $q = 2$.

For $q = 4$ (black squares) the $H^+ + H^+ + O^{2+}$ yield is the only relevant channel as reported in Ref. [17]. No MO IEM results were reported in Ref. [2]. The IAM-PCM result (green long-dashed line with crosses) overestimates the lower-energy experimental data by about a factor of 2. The energy dependence of the theoretical cross section is complicated in this range on account of the contribution of various multielectron processes. It may not match the experimental falloff very well, since autoionization contributions may be important at even lower energies than for $q = 3$ due to the smallness of the direct multiple removal contributions. The present IAM-PCM results are closer to experiment than the MO IEM results (which were not shown in Ref. [15], but which we include here for comparison).

Summarizing the findings reported in Fig. 2, we can state the the IAM-PCM is more successful than the MO IEM on account of the fact that it combines IEM calculations for proton collisions with constituent atoms (H and O in this case) for removal of one (or more) electrons to generate q-fold electron removal from the target molecule. As we observed in our previous work on ion collisions with multielectron targets (such as Ne [29], O [30], or Ar [31]), the IEM works reasonably well for processes that involve up to one more electron than the charge state of the projectile, i.e., two electrons in the case of proton impact. In the case of the H_2O target this is verified by good agreement for the $q = 2$ channel, but overestimation for $q = 3$ and failure for $q = 4$ when looking at MO IEM results. The comparison of the present $q = 1$–4 cross sections with the data of Ref. [17] shows that the energy dependence in the 100–350 keV range leads to a different slope in the double-logarithmic presentation with an apparent steepening of the curves as one goes through the sequence from $q = 1$ to $q = 4$. It would be useful in the future to have complete coincidence measurements at higher energies (such as those from Ref. [17]) in order to verify this behavior experimentally.

We now proceed to discuss an important objective of this work, namely, the application of Eq. (10) to calculate charge-state correlated cross sections within the IAM-PCM. In Fig. 3 the data for simultaneous capture of $k = 0, 1$ electrons and transfer of $l = 0, 1, 2, 3$ electrons to the continuum are presented for proton-water collisions. The capture channels are calculated according to $\tilde{\sigma}_{k,l}$ to avoid the fact that the trinomial evaluation within an IEM would predict unphysical multiple capture contributions (cf. Refs. [2,30]). As can be seen in Fig. 3, the net capture cross section is described very well within the IAM-PCM [8].

The pure ionization channels σ_{0l} can be compared to the experimental work of Ref. [20]. For the process where a single electron is produced in the continuum while the target fragmentation products together correspond to $q = 1$, i.e., no electron capture, this cross section σ_{01} is bounded from below by the H_2O^+ channel. The IAM-PCM result does obey this bound when compared to the experiment. The earlier data from Ref. [19] (not shown) are lower than those of Ref. [20] at the 10%–30% level and thus form a less tight bound.

For the process σ_{02}, i.e., pure double ionization, we can add the production cross sections for the fragmentation channels

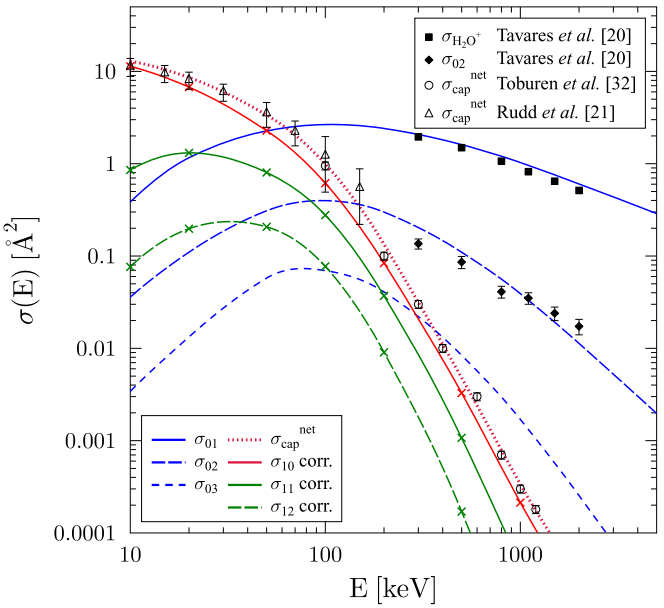

FIG. 3. Charge-state correlated cross sections σ_{kl} for proton collisions with water molecules versus impact energy. The IAM-PCM results are shown as curves: red solid line with crosses, pure single capture; green solid line with crosses, transfer ionization; green dashed line with crosses, transfer ionization with two electrons in the continuum; blue solid line, pure single ionization; blue dashed line, pure double ionization; blue short-dashed line, pure triple ionization. Shown as closed squares are the experimental pure single-ionization data (exclusively) for the H_2O^+ channel and as diamonds the pure double-ionization data from Tavares *et al.* [20] based on coincidence measurements $H^+ + OH^+$ and $H^+ + O^+$, but ignoring the $H^+ + H^+$ with neutral channel. The open symbols represent the derived net capture cross sections from experiments: circles, Toburen *et al.* [32]; triangles, Rudd *et al.* [21]. The red dotted line is the IAM-PCM net capture result [8].

$H^+ + OH^+$ and $H^+ + O^+$ shown in Fig. 4 and Table II of Ref. [20]. Assuming that the production of $H + H + O^{2+}$ is very small, the sum should yield a tight lower bound for this channel. Again, the IAM-PCM result agrees very closely with this bound. We note, however, that the proton-proton coincidence data of Werner *el al.* [17] show that the measurements of Ref. [20] do not provide the complete σ_{02} cross section, since the channel $H^+ + H^+$ with neutral (or negatively charged) oxygen atoms is a significant contributor which cannot be detected with the methodology of Ref. [20].

We note the markedly different energy dependence of the cross sections σ_{01} and σ_{02} at high energies. While the theoretical results for σ_{01} and σ_{02} energies above $E = 1$ MeV show $1/E$ and $1/E^2$ behavior, respectively, the experimental results indicate this for σ_{01}, but not for σ_{02}: While the first three data points follow the theory, the three higher ones indicate a turnover towards a weaker energy dependence. This could be caused by the onset of a competitive double-ionization process: electron removal from an inner molecular orbital leading to further autoionization. The present theoretical model does not include such a process. Eventually, at higher collision energies the autoionization process will dominate and σ_{02} follows the same energy dependence as σ_{01}.

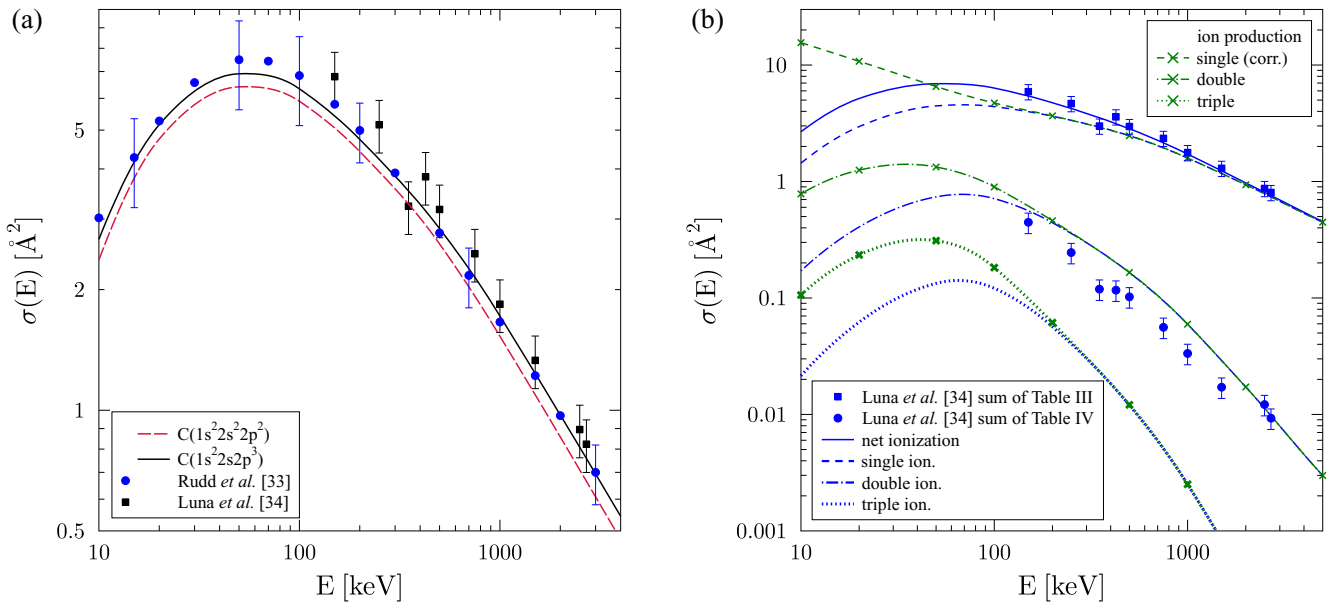

FIG. 4. (a) Net ionization cross section as a function of collision energy for proton-methane collisions. The present IAM-PCM calculation is based on the ground-state carbon atom [C($1s^2 2s^2 2p^2$)] input (red dashed line) and on the excited carbon atom [C($1s^2 2s 2p^3$)] input (black solid line). Experimental data are from Rudd *et al.* [33] (blue circles) and from Luna *et al.* [34] (black squares) which were normalized to the original measurements of Ref. [35]. (b) Total cross sections for l-fold ionization (σ_{0l} shown as blue curves) and total ion production (σ_q shown as green curves with crosses) as functions of impact energy in proton-methane collisions. Equations (15) and (16) are used to define the cross sections with electron capture which enter σ_q according to Eq. (17). The experimental data are from Luna *et al.* [34]. The squares denote $\sigma_1 \approx \sigma_{01}$ and the circles $\sigma_2 \approx \sigma_{02}$. The IAM-PCM results for net electron production (σ^-) are shown as a blue solid line, σ_{01} as a blue dashed line, and σ_1 as a green dashed line, followed by dash-dotted and dotted corresponding lines for the channels involving $l = 2, 3$ and $q = 2, 3$, respectively.

Our conclusion about the production mechanism for σ_{02} complements that presented in Ref. [20]. Based on the height of the cross section and its energy dependence, we would argue that pure double ionization (or $q = 2$ production at these energies) can be understood as a direct production mechanism, as discussed previously in Ref. [23]. Tavares *et al.* [20] at first argued that the near constancy of fragmentation ratios indicates that the channel may be generated by single ionization followed by autoionization at all energies, but in the end they also concluded from the energy dependence of the cross section that autoionization begins to play an important role only at energies above 1 MeV.

For the correlated capture processes (pure single capture and transfer ionization) no direct comparison with experiment can be provided since the projectile charge state needs to be detected in coincidence with the fragments. We can use the net capture cross sections at high energies from Ref. [32] and at lower energies from Ref. [21] to indicate that the sum of single capture σ_{10} and the transfer ionization channels σ_{11} and σ_{12} agrees well with this net cross section (as demonstrated in Ref. [8]). This net cross section (which in the literature is at times denoted by σ_{10} based on a different notation from our σ_{kl}) includes transfer ionization: It is formed by taking the difference of net recoil ion production σ^+ and net electron production σ^-. Take σ_{11} as an example: It enters σ^+ twice on account of $q = 2$ and σ^- once. Thus, the difference $\sigma^+ - \sigma^-$ contains σ_{11} once, and similar arguments hold for the higher-order transfer ionization processes.

B. $p + CH_4$ collisions

Figure 4 shows cross sections for ionization and total ion production in proton-methane collisions. The experimental total recoil ion production cross section for singly charged fragments is made up of contributions from many fragments, predominantly CH_4^+ and CH_3^+, followed by smaller contributions from CH_2^+, CH^+, and C^+. Production of H^+ is comparable in size to that of CH_2^+ [34]. Thus, the situation is more complex than for the water molecule. The normalization of the fragment cross sections reported by Luna *et al.* [34] is obtained with the help of previous coincidence measurements of Ben-Itzhak *et al.* [36], but is ultimately based on the original net ionization measurements of Rudd *et al.* [35]. In Fig. 4(a) these data (black squares) are compared to the subsequently recommended values of Rudd *et al.* [33], which are lower but within error bars (shown as blue circles).

Two results are offered within the IAM-PCM approach. Previously, σ^- and σ^+ were obtained within the method [7] based on the ground-state carbon C($1s^2 2s^2 2p^2$) configuration. Using an excited carbon configuration C($1s^2 2s 2p^3$), we obtain a higher result (black solid vs red dashed curve). This calculation reaches excellent agreement with the experimental data and is used for the subsequent analysis of multiple ionization. The justification for using an excited vs ground-state configuration of carbon to enter the IAM-PCM analysis is based on molecular modeling: A carbon atom cannot bind four ground-state hydrogen atoms when in the divalent C($1s^2 2s^2 2p^2$) configuration. For a discussion of the problem we refer the reader to Ref. [37].

The comparison of the solid and dashed lines in Fig. 4(b) shows the deviation between σ_1 and σ^-; at energies below $E = 100$ keV the cross sections for pure ionization fall, while the $q = 1$ production cross section rises due to capture contributions. The theoretical data are below the experimental data for low to intermediate energies, but part of the disagreement could also be a normalization issue.

The theoretical result for σ_{02} (blue dash-dotted line) is bounded from below by the experimental data of Ref. [34]. These data clearly support the notion of double ionization as a direct two-electron process, with an indication that for $E >$ 1000 keV autoionization is becoming a competitive process.

The absence of experimental data for $q = 3$ processes is a consequence of the procedure of coincidence counting of singly charged fragments in Ref. [34]. The fact that doubly charged fragments were not reported is also the reason why we treat the sum of experimental channels in Table IV of Ref. [34] as a lower bound to σ_q. The main contributions come from coincidences of H^+ with singly ionized hydrocarbons and carbon atoms. A natural channel for $q = 3$ production would be $H^+ + C^{2+}$, but no such data were reported.

For CH_4 a substantial amount of previous work, including coincidence measurements [36], made it clear that a $CH_4{}^{2+}$ channel leading to coincident charged decay products existed and had to be modeled [38]. The modeling carried out in Ref. [34] assumed that all produced $CH_4{}^{2+}$ molecules fragment into singly charged objects. Definitely missing in the experimental data for σ_{02} are coincidences of two protons, but in contrast to H_2O targets such a channel cannot contribute a large amount since overall H^+ production is relatively weak contributing on the order of 5%–6% only.

Capture processes (including transfer ionization) begin to play a role in ion production (σ_q) at energies below 200 keV, as indicated by the green curves with crosses (dashed for $q = 1$, dash-dotted for $q = 2$, and dotted for $q = 3$). We are not aware of experimental data that could be used to confirm these $q = 3$ results.

C. $p + NH_3$ collisions

In Fig. 5 we compare our predictions to the data of Ref. [39] for the ammonia target. In terms of the number of possible singly charged fragments ammonia is much richer than water but less prolific than methane: The singly charged fragment yields are strongly dominated by essentially equal amounts of $NH_3{}^+$ and $NH_2{}^+$. This is followed by H^+ production at the level of 6%–7% and then N^+ and some $H_2{}^+$. When comparing methane and ammonia one has to be aware of the fact that the stability of decay products in these systems is different. An interesting comparator is the observed presence of $NH_3{}^{2+}$, with no doubly charged hydrocarbons being recorded experimentally in the case of proton-methane collisions. For the normalization of the data, the recommendations for net cross sections from Ref. [33] were used.

This leads to a net cross section at high energies where $\sigma^+ \approx \sigma^- \approx \sigma_1$ and we observe that our IAM-PCM calculations show excellent agreement with this result over a wide range of energies. The situation compares well with the results for methane, for which a higher net cross section is obtained, namely, CH_4 is ionized more effectively than NH_3 by about

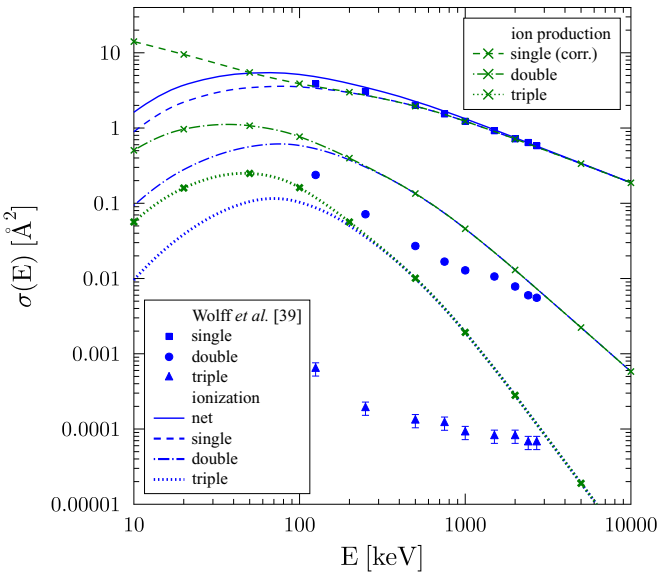

FIG. 5. Total cross sections for l-fold ionization (σ_{0l}) and total ion production (σ_q) as functions of impact energy in proton-ammonia molecule collisions. Equations (15) and (16) are used to define the cross sections with electron capture which enter σ_q according to Eq. (17). The experimental data are from Wolff *et al.* [39]. The squares denote $\sigma_1 \approx \sigma_{01}$, the circles $\sigma_2 \approx \sigma_{02}$, and triangles show $\sigma_3 \approx \sigma_{03}$. The IAM-PCM results for net electron production (σ^-) are shown as a blue solid line, σ_{01} as a blue dashed line, and σ_1 as a green dashed line with crosses, followed by dash-dotted and dotted corresponding lines for the channels involving $l = 2, 3$ and $q = 2, 3$ respectively.

40%, even though the number of available electrons is the same. Our model calculations show that half of this excess can be attributed to the fact that the carbon atom enters CH_4 in an excited configuration.

For double ionization we find remarkable disagreement between our results and the experimental data. The latter are obtained essentially by summing the coincidence counts of $H^+ + NH_2{}^+$, $H^+ + NH^+$, and $H^+ + N^+$, with some small contributions from $NH_3{}^{2+}$ and $NH^+ + H_2{}^+$. Doubly ionized nitrogen atoms were only found in coincidence with H^+, i.e., as part of the $q = 3$ channel [39]. This raises the question whether N^{2+} can be produced together with neutral hydrogen ($H_2{}^0 + H^0$ or $H^0 + H^0 + H^0$) without being detected.

Thus, we find that, compared to our prediction, the experimental $q = 2$ data show a markedly different energy dependence: They are lower than the theoretical results by a factor of 2 at 150 keV and then the discrepancy increases to about a factor of 4 at 400 keV. At higher energies the experimental data turn around to display an energy dependence that is comparable to the single-ionization cross section and they approach the theoretical values at the highest energies.

There are also experimental $q = 3$ data available for the ammonia target. The behavior with energy markedly disagrees with the theoretical results. This leads to the notion that $q = 2$ (and $q = 3$) production does not agree with an IEM, or the IAM, or that the measurements are incomplete and represent lower bounds to our data in the regions where direct multiple ionization should dominate.

In order to explain their data for NH_3 targets, Wolff *et al.* [39] resorted to a discussion based upon a correlated electron treatment of the molecular structure which was used to explain electron momentum spectroscopy data generated by electron impact [40]. This work showed that the details of these momentum spectra can be accounted for by going beyond the Hartree-Fock approximation using configuration-interaction methods. On the other hand, the same apparently applies to the water molecule, for which such an analysis was reported in Ref. [41]. To analyze their data Wolff *et al.* construct a phenomenological fragmentation model to deal with single ionization, while discarding multiple-ionization effects.

To summarize this section we note the anomalous behavior we found for the ammonia molecule target. For H_2O we find agreement with experiments that are sensitive to channels $q = 1$–4. For CH_4 we have consistent results with experiment for $q = 1, 2$. Why this should not apply to NH_3 as well remains a mystery at present. One way to look into this mystery would be a study by coincidence techniques that can detect proton-proton coincidences, such as the methodology of Ref. [17]. An additional approach would be to check the coincidence channel for electrons with doubly charged atoms to be sensitive to processes where neutral atoms or molecules are produced together with doubly charged fragments.

IV. CONCLUSION

We have presented a formalism for IAM calculations to evaluate cross sections for charge-state correlated processes in ion-molecule collisions, which can then be summed to form partially inclusive cross sections, such as q-fold electron removal. Application of the IAM-PCM to three molecules consisting of ten electrons, where one would expect similar results for multiple ionization, led to different conclusions for the three cases. While comparison with coincidence data for proton collisions with water molecules agreed favorably for a multiple-ionization approach, the agreement was confirmed for methane only at the level of $q = 1, 2$. One might argue that the applied coincidence technique was limited and could not detect the simultaneous emission of two (or more) protons [34], something which was available in the work of Werner *et al.* for the water target [17]. The case of the ammonia target led, however, to a bigger puzzle, since in this case even the direct $q = 2$ multiple-ionization channel turned out to be rather weak, i.e., a shortfall by a factor of about 4–5 at intermediate energies.

From a modeling perspective this is puzzling, since the three target molecules theoretically have similar vertical ionization energies. Using the geometry of the neutral molecule, these energies (calculated with Hartree-Fock or a correlated coupled-cluster method [42]) roughly scale as $0.45q$ a.u. (at the $\pm 10\%$ level based on structure calculations for $q = 0, \ldots, 3$) and should thus be equally amenable to an IAM approach in the high collision energy limit. On the other hand, the similarity of the ionization energies can be contrasted with differences in the electronic configurations such as the number of bonding and nonbonding orbitals in the three molecules. While it is not obvious how this might affect the multiple-ionization yields, it is certainly a feature beyond the present IAM description.

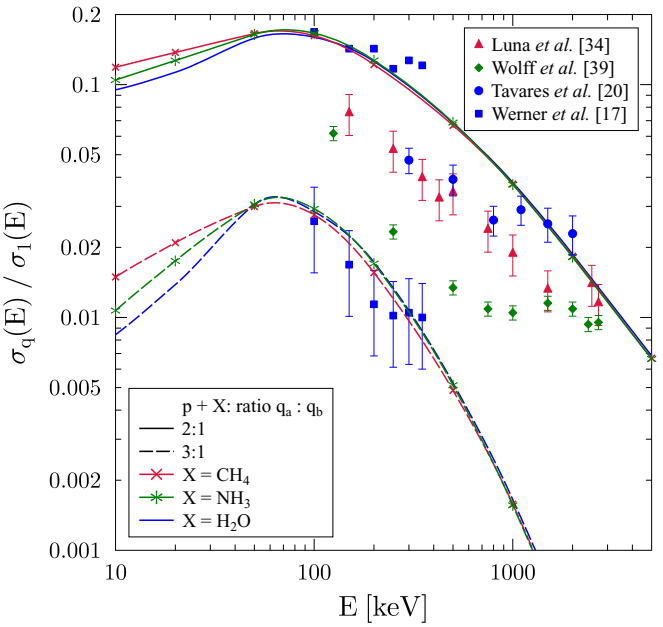

FIG. 6. Ratios of q-fold electron removal cross sections σ_2/σ_1 (solid lines) and σ_3/σ_1 (dashed lines) vs energy as calculated in the IAM-PCM approach for proton collisions with water (blue), methane (red with crosses), and ammonia (green with asterisks) collisions. Experiments with H_2O are from Werner *et al.* [17] (blue squares) and Tavares *et al.* [20] (blue circles), with CH_4 are from Luna *et al.* [34] (red triangles), and with NH_3 are from Wolff *et al.* [39] (green diamonds).

The scaling of the IAM-PCM data is shown in Fig. 6 in the form of ratios of cross sections σ_2/σ_1 and σ_3/σ_1 comparing the three molecular targets. The theoretical results differ for the molecules at energies below 100 keV only and merge into universal curves for high energies. For σ_2/σ_1 an energy dependence of $\ln(E)/E$ is observed and as expected for $\sigma_3/\sigma_1 \sim [\ln(E)/E]^2$. Unexpected is the observation of a universal curve for the three targets, since the constituent atoms have their own dependences. The experimental data for the water target (blue symbols) agree with the finding at intermediate energies with the σ_2/σ_1 data of Ref. [20] being on the low side by comparison at intermediate energies and then indicating a turnover to a constant at high energies due to autoionization becoming the dominant process for $q = 2$.

The ratio σ_3/σ_1 agrees well with the measurements of Ref. [17]. The experimental σ_2/σ_1 data for methane follow the expected $\ln(E)/E$ trend over a wide range, but are lower by a factor of 2, and no data are given for σ_3/σ_1.

For the ammonia target the experimental results for σ_2/σ_1 display a very steep and counterintuitive falloff for the first three data points and then turn over to a constant. We do not show the experimental ratio σ_3/σ_1, since it would be below our bottom scale end. The ratio is of the order of 10^{-4} (cf. Fig. 5) and actually increase with E for large energies.

These observations lead to the conclusion that the IAM-PCM approach is very strong in predicting net cross sections (dominated by the $q = 1$ removal cross sections), but need to be tested on a case by case basis for the higher-q

predictions. Discrete electronic excitations of the investigated molecules can also lead to fragmentation [43] and may also show different behavior among them. Further experimental work on such molecules containing multiple hydrogen bonds, especially experiments capable of proton-proton coincidences, are needed to resolve some of the remaining questions of this work.

ACKNOWLEDGMENTS

We would like to thank the Center for Scientific Computing, University of Frankfurt for making their High Performance Computing facilities available. Financial support from the Natural Sciences and Engineering Research Council of Canada (Grants No. RGPIN-2017-05655 and No. RGPIN-2019-06305) is gratefully acknowledged.

[1] *Radiation Damage in Biomolecular Systems*, edited by G. García Gómez-Tejedor and M. C. Fuss (Springer, Dordrecht, 2012).

[2] M. Murakami, T. Kirchner, M. Horbatsch, and H. J. Lüdde, Phys. Rev. A **85**, 052704 (2012).

[3] A. Salehzadeh and T. Kirchner, Eur. Phys. J. D **71**, 66 (2017).

[4] A. Jorge, M. Horbatsch, and T. Kirchner, Phys. Rev. A **102**, 012808 (2020).

[5] H. J. Lüdde, M. Horbatsch, and T. Kirchner, Eur. Phys. J. B **91**, 99 (2018).

[6] H. J. Lüdde, M. Horbatsch, and T. Kirchner, J. Phys. B **52**, 195203 (2019).

[7] H. J. Lüdde, M. Horbatsch, and T. Kirchner, Eur. Phys. J. D **73**, 249 (2019).

[8] H. J. Lüdde, A. Jorge, M. Horbatsch, and T. Kirchner, Atoms **8**, 59 (2020).

[9] H. J. Lüdde, T. Kalkbrenner, M. Horbatsch, and T. Kirchner, Phys. Rev. A **101**, 062709 (2020).

[10] H. J. Lüdde, in *Many-Particle Quantum Dynamics in Atomic and Molecular Fragmentation*, edited by J. Ullrich and V. P. Shevelko (Springer, Berlin, 2003), pp. 205–220.

[11] M. Horbatsch, Phys. Rev. A **49**, 4556 (1994).

[12] D. R. Schultz, R. E. Olson, C. O. Reinhold, S. Kelbch, C. Kelbch, H. Schmidt-Böcking, and J. Ullrich, J. Phys. B **23**, 3839 (1990).

[13] M. E. Rose, *Elementary Theory of Angular Momentum* (Dover, Mineola, 1995).

[14] M. Zapukhlyak, T. Kirchner, H. J. Lüdde, S. Knoop, R. Morgenstern, and R. Hoekstra, J. Phys. B **38**, 2353 (2005).

[15] M. Murakami, T. Kirchner, M. Horbatsch, and H. J. Lüdde, Phys. Rev. A **85**, 052713 (2012).

[16] T. Kirchner, M. Murakami, M. Horbatsch, and H. J. Lüdde, Adv. Quantum Chem. **65**, 315 (2013).

[17] U. Werner, K. Beckord, J. Becker, and H. O. Lutz, Phys. Rev. Lett. **74**, 1962 (1995).

[18] F. Gobet, S. Eden, B. Coupier, J. Tabet, B. Farizon, M. Farizon, M. J. Gaillard, M. Carré, S. Ouaskit, T. D. Märk, and P. Scheier, Phys. Rev. A **70**, 062716 (2004).

[19] H. Luna, A. L. F. de Barros, J. A. Wyer, S. W. J. Scully, J. Lecointre, P. M. Y. Garcia, G. M. Sigaud, A. C. F. Santos, V. Senthil, M. B. Shah, C. J. Latimer, and E. C. Montenegro, Phys. Rev. A **75**, 042711 (2007).

[20] A. C. Tavares, H. Luna, W. Wolff, and E. C. Montenegro, Phys. Rev. A **92**, 032714 (2015).

[21] M. E. Rudd, T. V. Goffe, R. D. DuBois, and L. H. Toburen, Phys. Rev. A **31**, 492 (1985).

[22] G. H. Olivera, C. Caraby, P. Jardin, A. Cassimi, L. Adoui, and B. Gervais, Phys. Med. Biol. **43**, 2347 (1998).

[23] L. Gulyás, S. Egri, H. Ghavaminia, and A. Igarashi, Phys. Rev. A **93**, 032704 (2016).

[24] P. N. Terekhin, M. A. Quinto, J. M. Monti, O. A. Fojón, and R. D. Rivarola, J. Phys. B **51**, 235201 (2018).

[25] C. Illescas, L. F. Errea, L. Méndez, B. Pons, I. Rabadán, and A. Riera, Phys. Rev. A **83**, 052704 (2011).

[26] N. Bachi, S. Otranto, G. S. Otero, and R. E. Olson, Phys. Med. Biol. **64**, 205020 (2019).

[27] A. Bhogale, S. Bhattacharjee, M. R. Chowdhury, C. Bagdia, M. F. Rojas, J. M. Monti, A. Jorge, M. Horbatsch, T. Kirchner, R. D. Rivarola, and L. C. Tribedi, Phys. Rev. A **105**, 062822 (2022).

[28] K. Tan, C. Brion, P. Van der Leeuw, and M. van der Wiel, Chem. Phys. **29**, 299 (1978).

[29] T. Kirchner, M. Horbatsch, H. J. Lüdde, and R. M. Dreizler, Phys. Rev. A **62**, 042704 (2000).

[30] T. Kirchner, H. J. Lüdde, M. Horbatsch, and R. M. Dreizler, Phys. Rev. A **61**, 052710 (2000).

[31] T. Kirchner, M. Horbatsch, and H. J. Lüdde, Phys. Rev. A **66**, 052719 (2002).

[32] L. H. Toburen, M. Y. Nakai, and R. A. Langley, Phys. Rev. **171**, 114 (1968).

[33] M. E. Rudd, Y. K. Kim, D. H. Madison, and J. W. Gallagher, Rev. Mod. Phys. **57**, 965 (1985).

[34] H. Luna, W. Wolff, E. C. Montenegro, and L. Sigaud, Phys. Rev. A **99**, 012709 (2019).

[35] M. E. Rudd, R. D. DuBois, L. H. Toburen, C. A. Ratcliffe, and T. V. Goffe, Phys. Rev. A **28**, 3244 (1983).

[36] I. Ben-Itzhak, K. D. Carnes, D. T. Johnson, P. J. Norris, and O. L. Weaver, Phys. Rev. A **49**, 881 (1994).

[37] F. Wang, J. Mol. Struct.: THEOCHEM **678**, 105 (2004).

[38] H. Luna, E. G. Cavalcanti, J. Nickles, G. M. Sigaud, and E. C. Montenegro, J. Phys. B **36**, 4717 (2003).

[39] W. Wolff, H. Luna, E. C. Montenegro, and L. C. Rodrigues Junior, Phys. Rev. A **102**, 052821 (2020).

[40] A. Bawagan, R. Müller-Fiedler, C. Brion, E. Davidson, and C. Boyle, Chem. Phys. **120**, 335 (1988).

[41] A. Bawagan, C. Brion, E. Davidson, and D. Feller, Chem. Phys. **113**, 19 (1987).

[42] J. M. Montgomery and D. A. Mazziotti, J. Chem. Educ. **97**, 3658 (2020).

[43] M. Danko, J. Orszagh, M. Ďurian, J. Kočišek, M. Daxner, S. Zöttl, J. B. Maljković, J. Fedor, P. Scheier, S. Denifl, and Š. Matejčík, J. Phys. B **46**, 045203 (2013).